Conference Proceedings of the Society for Experimental Mechanics Series

Eann Patterson · David Backman · Gary Cloud *Editors*

Composite Materials and Joining Technologies for Composites, Volume 7

Proceedings of the 2012 Annual Conference on Experimental and Applied Mechanics

SEM Springer

Conference Proceedings of the Society for Experimental Mechanics Series

Series Editor
Tom Proulx
Society for Experimental Mechanics, Inc.,
Bethel, CT, USA

For further volumes:
http://www.springer.com/series/8922

Eann Patterson • David Backman • Gary Cloud
Editors

Composite Materials and Joining Technologies for Composites, Volume 7

Proceedings of the 2012 Annual Conference on Experimental and Applied Mechanics

Springer

Editors
Eann Patterson
University of Liverpool
UK

David Backman
National Research Council Canada
Ottawa, ON, Canada

Gary Cloud
Michigan State University
East Lansing, MI, USA

ISSN 2191-5644 ISSN 2191-5652 (electronic)
ISBN 978-1-4614-4552-4 ISBN 978-1-4614-4553-1 (eBook)
DOI 10.1007/978-1-4614-4553-1
Springer New York Heidelberg Dordrecht London

Library of Congress Control Number: 2012945402

Printed on acid-free paper

Springer is part of Springer Science+Business Media (www.springer.com)

Preface

Composite Materials and Joining Technologies for Composites, Volume 7: Proceedings of the 2012 Annual Conference on Experimental and Applied Mechanics represents one of seven volumes of technical papers presented at the Society for Experimental Mechanics SEM 12th International Congress & Exposition on Experimental and Applied Mechanics, held at Costa Mesa, California, June 11–14, 2012. The full set of proceedings also includes volumes on Dynamic Behavior of Materials, Challenges in Mechanics of Time-Dependent Materials and Processes in Conventional and Multifunctional Materials, Imaging Methods for Novel Materials and Challenging Applications, Experimental and Applied Mechanics, Mechanics of Biological Systems and Materials, and MEMS and Nanotechnology.

Each collection presents early findings from experimental and computational investigations on an important area within Experimental Mechanics. The Composite Materials and the first International Symposium on Joining Technologies for Composites conference track was organized by Eann Patterson, University of Liverpool; David Backman, National Research Council Canada; Gary Cloud, Michigan State University; and sponsored by the SEM Composite Materials Technical Division.

As composite materials have moved from smaller-scale applications to wider acceptance in larger-scale application areas such as automotive or aerospace structures, the need for improved joining of composites has become increasingly important. Composite joining technologies in the past have been widely grouped into mechanical joining or adhesive joining. Increasingly, joint optimization has required combinations of the two methods as well as introducing innovative new methods such as composite welding that provide high strength and light weight. Today, developments in composite joining technologies are being made at a rapid rate, driven by both technology and user requirements.

To provide a forum for an up-to-date account of the advances in the field of composite joining technologies and to promote an alliance between governmental, industrial, and academic practitioners, SEM has agreed to initiate a *Symposium Series on Joining Technologies for Composites*. The 2012 Symposium will be the first of a potential series and will address pertinent issues relating to design, analysis, fabrication, testing, optimization, reliability, and applications of composite joints, especially as these issues relate to experimental mechanics of both the macroscale and microscale structures.

Topics included in this volume are:

Composite Joining for Heavy Duty Applications
Advances in Fastening and Joining
Modeling and Validation of Composite Joints
Composite Joints in Aerospace Related Applications
Fatigue and Fracture of Composite Joints
Composite Characterization using Digital Image Correlation Techniques
Nanocomposites for Improved Composite Performance
Impact Behavior of Composites

The contribution of the organizing committee, session chairs, authors and keynote speakers is gratefully acknowledged along with the support from SEM staff.

The opinions expressed herein are those of the individual authors and not necessarily those of the Society for Experimental Mechanics, Inc.

Liverpool, UK — Eann Patterson
Ottawa, ON, Canada — David Backman
East Lansing, MI, USA — Gary Cloud

Contents

1 **Evaluating Bolted Joint Strength at High Strain Rates** 1
Srinivasan Arjun Tekalur, Andy VanderKlok, Wei Zhang, and Abhishek Dutta

2 **Fastening and Joining of Composite Materials** 5
Sayed A. Nassar and Xianjie Yang

3 **Inter-cellular Joining for Amorphous Honeycombs** 25
Balaji Jayakumar, Masoud Allahkarami, and Jay C. Hanan

4 **Milled Glass Reinforced Polyurea Composites: The Effect of Surface Treatment** 35
Zhanzhan Jia, Kristin Holzworth, and Sia Nemat-Nasser

5 **Experimental and Numerical Characterization of Relaxation in Bolted Composite Joints** 39
Ronald F. Gibson and Srinivasa D. Thoppul

6 **New Composite Timbers, Full Field Analysis of Adhesive Behavior** 51
Boris Clouet, Régis Pommier, and Michel Danis

7 **Cylindrical Bending of Bonded Layered Thick Composites** 59
Sayed A. Nassar, Jianghui Mao, Xianjie Yang, and Douglas Templeton

8 **A Novel Method to Attach Membranes Uniformly on MAV Wings** 71
Yaakov J. Abudaram, Sean Rohde, James Paul Hubner, and Peter Ifju

9 **A Model for Fracture Characterization of Adhesively-Bonded Joints** 81
Jianghui Mao, Sayed A. Nassar, and Xianjie Yang

10 **Probabilistic Characterization of Elastic Properties of Composites Using Digital Image Correlation Technique** 93
Mark R. Gurvich and Patrick L. Clavette

11 **Mechanics of Fiber-Reinforced Porous Polymer Composites** 99
Sandip Haldar and Hugh A. Bruck

12 **Mechanics of Multifunctional Skin Structures** 107
Hugh A. Bruck, Kelsey Cellon, Satyandra K. Gupta, Mark Kujawski, Ariel Perez-Rosado, Elisabeth Smela, and Miao Yu

13 **Non-local Damage-Enhanced MFH for Multiscale Simulations of Composites** 115
Ling Wu, Ludovic Noels, Laurent Adam, and Issam Doghri

14 **Composite Damage Detection with Self-Sensing Fibers and Thermal Sprayed Electrodes** 123
Toshio Nakamura and Masaru Ogawa

15 **Experimental Investigation of Fatigue Behavior of Carbon Fiber Composites Using Fully Reversed Four Point Bending Test** 131
A. Amiri and M.N. Cavalli

16 Spark Plasma Sintering and Characterization of Graphene Reinforced Silicon Carbide Nanocomposites 139
Arif Rahman, Ashish Singh, Sandip P. Harimkar, and Raman P. Singh

17 Processing, Microstructure, and Properties of Carbon Nanotube Reinforced Silicon Carbide 147
Thomas A. Carlson, Charles P. Marsh, Waltraud M. Kriven, Peter B. Stynoski, and Charles R. Welch

18 HP/HT Hot-Wet Resistance of Thermoplastic PEEK and Its Composites 161
Yusheng Yuan, Jim Goodson, and Rihong Fan

19 Reinforcement of Epoxy Resins with POSS for Enhancing Fracture Toughness at Cryogenic Temperature 179
Kunal Mishra and Raman P. Singh

20 Ballistic Impact Behaviors of GLARE 5 Fiber-Metal Laminated Plates 189
A. Seyed Yaghoubi and B. Liaw

21 Impact of Aluminum, CFRP Laminates, Fibre-Metal Laminates and Sandwich Panels 199
Shengqing Zhu and Gin Boay Chai

22 Impact Monitoring in Aerospace Panels via Piezoelectric Rosettes 207
Francesco Lanza di Scalea, Hyonny Kim, Sara White, Zhi M. Chen, Salvatore Salamone, and Ivan Bartoli

23 Using Experimental Data to Improve Crash Modeling for Composite Materials 215
Morteza Kiani, Hirotaka Shiozaki, and Keiichi Motoyama

24 Design of New Elastomeric Matrix Composites: Comparison of Mechanical Properties and Determining Viscoelastic Parameters via Continuous Micro Indentation 227
D. Zaimova, E. Bayraktar, G. Berthout, and N. Dishovsky

25 Polyurea-Based Composites: Ultrasonic Testing and Dynamic Mechanical Properties Modeling 235
Wiroj Nantasetphong, Alireza V. Amirkhizi, Zhanzhan Jia, and Sia Nemat-Nasser

Chapter 1
Evaluating Bolted Joint Strength at High Strain Rates

Srinivasan Arjun Tekalur, Andy VanderKlok, Wei Zhang, and Abhishek Dutta

Abstract Experimental evaluation of bolted joint strength at high strain rates is a challenging but vital research. In the current study, a single lap bolted joint is studied using a Split Hopkinson Bar Pressure setup. The objective of the study is to understand the effect of variable geometrical parameters in the single lap bolted joint experimentally. Subsequently, only those aspects of these parameters that can confine to the dynamic experimental technique are selected. The challenges of the setup, the role of equilibrium and the occurrence of buckling are all studied critically to understand what is the best method to evaluate the joint strength under impact/high strain rate loading conditions.

Keywords Monolithic joint • Split hopkinson pressure bac • Equilibrium

1.1 Introduction

Bolted joints is a simple way to attach two structures together, and at the same time allows for a non-destructive means to separate the structures for repair or maintenance. This method of fastening has been extensively tested in the static to quasi-static regime with cross head speeds of 0.1–10 mm/s, but has been neglected at even higher rates of loading [1]. Static testing has been extensively carried out in both bearing and tensile configuration. Within the bearing configuration the primary modes of failure are considered to be out of plane buckling and hole elongation. Both failure modes are highly dependent upon geometrical parameters of the specimen. Results for static bearing testing show a trend for increasing diameter by thickness (d/t) yields lower ultimate bearing strength. Similarly, for edge by diameter (e/d) and width by diameter w/d show an asymptotic region where failure mode abruptly changes from shear at low stress to buckling at higher stresses. This asymptotic region of failure mode alteration is common in both the geometrical parameters e/d and w/d for bearing and tensile loading configuration, and occurs at a ratio of approximately 3.0 [2] [3]. This asymptotic behavior is has been extensively tested in the static regime where shear failure is abruptly changed to buckling for a certain e/d, w/d, and d/t ratio. The aim of this paper is to determine if any such behavior is present at high loading rates for monolithic specimens, along with subsequent determination of an optimal geometry for SHPB testing of bolted joints.

Most failures of bolted structures are predominant when loading acting on the structure is dynamic in nature thereby, motivating the need for further research on the behavior of bolted joints under impact rates of loading. In this paper we introduce the preliminary steps involved testing bolted joints in a split Hopkinson pressure bar at loading rates of approximately 500 MN/s.

This involves satisfying equilibrium and buckling conditions by testing a set of monolithic specimens with varying length and widths to determine optimum geometric parameters only. A finite element model had been constructed using ABAQUS to mimic the behavior of the experimentally tested monolithic specimens. This model was verified to match trends of monolithic specimen loading rate, equilibrium time, and equilibrium start time for a fixed $d/t = 1$, $w/d = 2.83$, and varying $e/d = 1,2,3$, and 4. Validation of the FEM against experimentally obtained results ensures the application of the model to

S.A. Tekalur (✉) • A. VanderKlok • W. Zhang • A. Dutta
Department of Mechanical Engineering, Michigan State University, 2727 Alliance Drive, Lansing, MI 48910, USA
e-mail: tsarjun@egr.msu.edu

E. Patterson et al. (eds.), *Composite Materials and Joining Technologies for Composites, Volume 7: Proceedings of the 2012 Annual Conference on Experimental and Applied Mechanics,* Conference Proceedings of the Society for Experimental Mechanics Series 44,
DOI 10.1007/978-1-4614-4553-1_1,

determine monolithic specimen behavior for other geometries that are not restrained by the diameter of the SHPB apparatus. Finally, an optimal geometry can be determined for ideal bolted joint testing where failure due to buckling and equilibrium times of specimen will be well established.

1.2 Materials and Methods

Testing of monolithic specimens was conducted using a Split Hopkinson Pressure Bar (SHPB) apparatus. The configuration utilizes 0.75 in. 6,061 Aluminum incidence and transmission bars with electro-resistive strain gages diametrically opposing centrally placed on each bar. The incident pulse was generated using a 5 in. striker powered by 30 psi of compressed Helium. For specimen equilibrium to be obtained, and to limit dispersive effects such as Pochhammer-Cree oscillations a pulse shaping material was employed between the striker and incidence bar [4]. Data acquisition system consists of an Ectron amplifier E513-2A with circuitry configured for half bridge and Lecroy Wave Jet 354A oscilloscope. Monolithic specimens that are geometrically similar to a uniaxial loaded bolted joint configuration were prepared with a fixed d/t = 1, w/d = 2.83, and varying e/d = 1, 2, 3, and 4. For each e/d ratio five specimens were manufactured, and four of each was tested with one spare for any specimen that may have been lost during testing. Experimental results show 95% confidence error bars for 4 specimens. The FEM results show an average of 5 calculations of the same e/d configuration to reduce the bias of human calculation of takeoff and landing of incident, reflected, and transmission waves. The FEM model was constructed with ABAQUS (version 6.9–2) and contains an incident and transmission bar. An input pulse directly from experimental data was used for the system excitation. Using an element in the center of the incident and transmission bar within the model, the incident, reflected, and transmission waves were extracted for analysis of equilibrium times and loading rate similarly to the experiment (Fig. 1.1a).

Table 1.1 shows the geometrical parameters non-dimensionalized with respect to a hole diameter. It is important to note that the hole diameter is a fictitious value as there is no hole in the monolithic specimen. Each specimen was loaded into the SHPB setup where incidence, reflected, and transmission waves were recorded for computation of loading rate, total equilibrium time, and equilibrium start time. Parameters of w/d and e/d were fixed as the SHPB apparatus restrains from any larger specimens.

1.3 Results

Specimen geometries were altered according to Table 1.1 and incident, reflected, and transmitted waves recorded for each test. Using one dimensional wave theory and Eqs. 1.1 and 1.2 Figs. 1.2 and 1.3 were constructed to determine optimal specimen properties for later testing of bolted joints of similar dimensions. The force on the transmission face was calculated using Eq. 1.2 where the slope of the transmitted pulse was used to calculate the loading rate of the specimen. Five FEM simulations for e/d of 1 and 4 were run using ABAQUS and averaged to smooth any outliers in the data due to the human

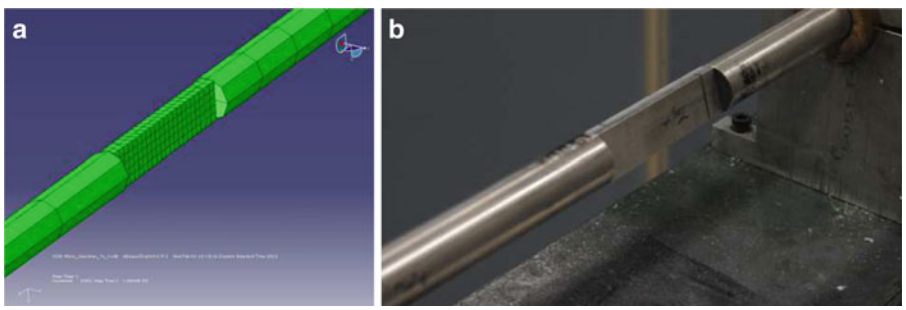

Fig. 1.1 ABAQUS model with specimen 4 ready to be tested (**a**) and the experimental setup (**b**) with the specimen sandwiched between the incident and transmission bars

Table 1.1 Geometric parameters for monolithic specimen testing

Specimen #	1	2	3	4
e/d	1.00	2.00	3.00	4.00
l/d	4.50	6.50	8.50	10.50

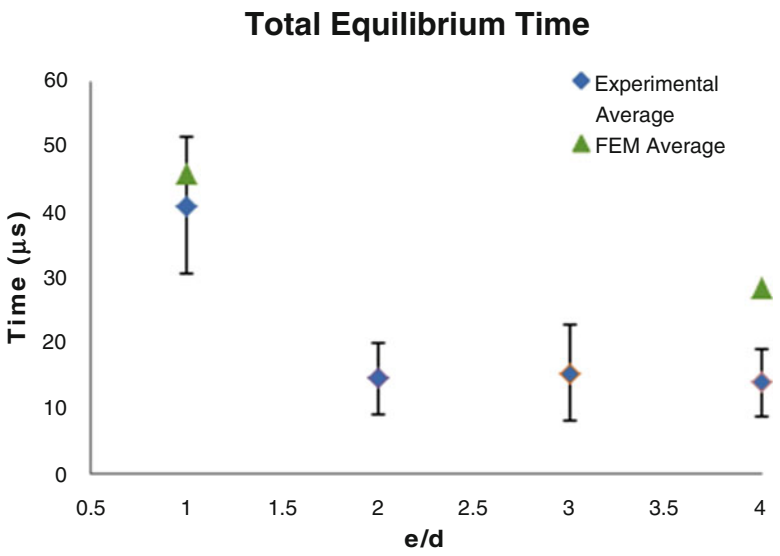

Fig. 1.2 Total amount of time the specimen is at equilibrium for varying e/d in compression. Experimental error bars are calculated with 95% confidence interval

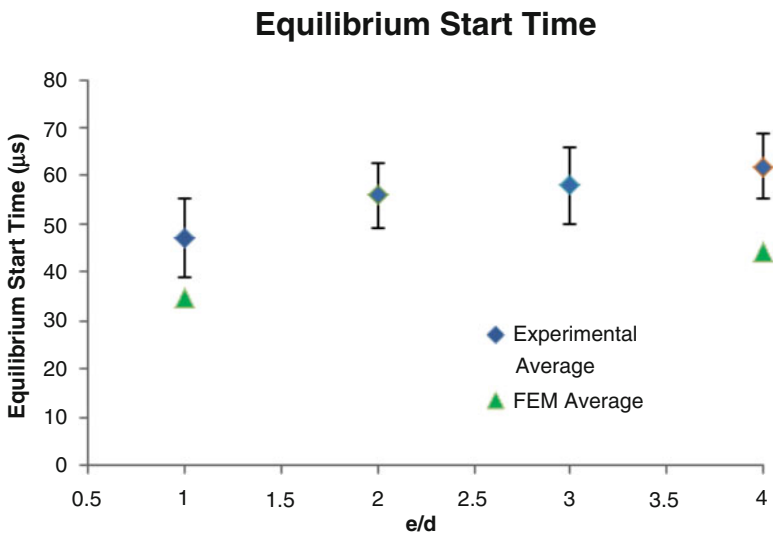

Fig. 1.3 The amount of time it takes the specimen to first reach equilibrium for varying e/d in compression. Experimental error bars are calculated with 95% confidence interval

interface between where to select where each pulse begins and ends. The general trend of the loading rate shows a slight increase from 450 MN/s to approximately 600MN/s as specimen e/d increase. Calculation of equilibrium times was conducted using both the force on the incident and transmission sides of the specimen. Plotting the incidence by transmission on the y-axis and time on the x-axis; equilibrium occurs when this force ratio is at unity. From this plot the total equilibrium time of the specimen can be obtained as well as when the specimen first reaches equilibrium as shown in Figs. 1.2 and 1.3 respectively.

1.4 Discussion

Using one dimensional wave propagation wave theory for elastic solids the following relations is established to determine loading rate, and equilibrium times [5].

$$F_{\text{inc.}}(t) = \text{A}_{\text{inc.bar}} E_{\text{bar}} (\varepsilon_{\text{i}}(t) + \varepsilon_r(t)) \tag{1.1}$$

$$F_{\text{trans.}}(t) = \text{A}_{\text{trans.bar}} E_{\text{bar}} (\varepsilon(t)) \tag{1.2}$$

Where $F_{inc.}$ and $F_{trans.}$ are the force on the incident and transmitted face of the SHPB. $A_{inc.bar}$ and $A_{trans.bar}$ is the cross-sectional area of the incident and transmission bars respectively. E_{bar} is the elastic modulus of the bars, and ε_i, ε_r, and ε_t are the recorded incident, reflected, and transmitted strain pulses from the adhesively bonded strain gages on the SHPB. Using split Hopkinson bar wave theory, specimen loading rate and equilibrium times can be calculated. This combined with visually inspecting each monolithic specimen for any mode of buckling will ensure proper specimen geometry for bolted joint testing in a SHPB setup.

Ideal specimen properties are high total equilibrium times, low equilibrium start times and low chances of buckling or bending. In the literature [4], it can be seen that equilibrium typically occurs at approximately 17–20 μs for sample lengths of 0.76–1.5 mm in length respectively. Length of the tested monolithic specimens varied from 1.125 to 2.875in (73.025 mm). For range of specimen length, it can be seen that the equilibrium start time is much higher, ranging from 45 to 63 μs due to inertia and non-uniform deformation due to wave propagation effects [4]. The increase in equilibrium start time is dependent on the length and inertia of the specimen as the longer specimen requires more time for the pulse to propagate through the specimen. As only a finite incidence pulse is generated tradeoff occurs between total time spent in equilibrium and equilibrium start times. This effect can be noticeably seen at e/d ratio of approximately 2.5. This behavior reflects nicely with the amount of specimens recorded as bent or deformed during testing with a decrease in total time spent in equilibrium. The FEM results follow closely to the actual experimental results in that general trends are still kept precise. However the accuracy of the model shows that some assumptions made in the model need to be refined. This error is mostly introduced between the interface between the specimen, incidence, and transmission bars has been modeled to be in perfect slip contact. This can cause the model to underestimate the actual equilibrium start time and over estimate the total time spent at equilibrium.

1.5 Conclusion

From the collected data it can be deduced that there does exist an optimum bolted joint geometry that can reach equilibrium and avoid local bending. Figures 1.2 and 1.3 show that increasing a specimen length will decrease the chance of buckling or local bending to occur, at the same time there exists a geometry where minimal local bending takes place with relatively high equilibrium times. The ideal bolted joint parameters that would yield the best result would be e/d = 2.0 or total length of 1.625 in. for minimal local bending and maximum time spent at equilibrium for a dynamic loading rate of approximately 500 MN/s. Upon identification of the critical e/d ratio, future work would include varying w/d and d/t parameters to identify where failure behavior of the joint would no longer be dominated by buckling.

References

1. Pearce GM, Johnson AF, Thomson R, Kelly DW (2010) Experimental investigation of dynamically loaded bolted joints in carbon fibre composite structures. Appl Compos Mater 17:271–291
2. Kretsis G, Matthews F (1985) The strength of bolted joints in glass fibre/epoxy laminates. Composites 16(2):92–102
3. Smith P, Pascoe K, Polak C, Stroud D (1986) The behaviour of single-lap bolted joints in CFRP laminates. Compos Struct 6:41–55
4. Wu X, Gorham D (1997) Stress equilibrium in the split Hopkinson pressure bar test. J Phys 7:C3-91–C3-96
5. Kolsky H (1949) An investigation of the mechanical properties of materials at very high rates of loading. Proc Phys Soc 62:C3-91–C3-96

Chapter 2
Fastening and Joining of Composite Materials

Sayed A. Nassar and Xianjie Yang

Abstract This paper presents some of the most recent advances in fastening and joining research on composite joints, which are often viewed as the weakest links that can significantly affect the safety and reliability of many mechanical and structural systems. A system approach is outlined for fastening and joining issues, which includes the effect of six groups of variables; namely, the joint, the joining element, tool used, process control, in-service loads, and the environmental variables. Challenging bolting issues are discussed as they apply to composite joints that are subjected to complex mechanical, thermo-mechanical, and environmental loading. This includes theoretical, FEA, and experimental models for investigating the effect of bolt holes, failure modes, vibration and impact-induced loosening of preloaded threaded fasteners, loss of clamp load due to mismatched thermal effects, and elastic interaction. Investigated joining variables in layered joints include normal and interfacial stresses, properties and thickness of the adhesive layers, additives, and damage modeling. Results from theoretical and experimental models are presented.

Keywords Composite materials • Composite joining • Bolted composites • Adhesive joined composites

2.1 Introduction

Composite materials have recently become more desirable for use in mechanical and structural components due to their relatively high specific strength and stiffness-to-weight ratios. Composites can also be designed and optimized to meet different strength and stiffness requirement in various directions as dictated by the design and performance of a structural component. Unlike metallic structures, the modeling and analysis of composite structures is a fairly challenging task. The load-carrying capacity of the composite material continues to be severely limited by the reduced load carrying capacity at the joint or attachment locations to the main structure. Due to anisotropy and inhomogeneity of composites, their response to loading is more complex, as compared to metallic structures. For a reliable design of composite structures, it is essential to thoroughly understand their behavior under static and dynamic mechanical and thermal loading under various environmental scenarios during the life of the component. The development of such design methods must be based on test data, analytical and computer modeling as well as numerical models using Finite Elements techniques.

The fastening and joining of composite materials mainly consist of the bonding and mechanical fastening. The main objective of bolted joints is to transfer applied load from one part of the joint structure to the other through fastener elements. However, bolt holes cause a stress concentration in the composite joint plates, which can severely reduce the mechanical strength and fatigue life of the joined structures. There are several possible joint failure modes in composites and three of the common ones are bearing, net tension and shear-out. Among them, bearing failure is often considered as the "desirable" mode because it usually gives a higher strength and the failure is less brittle. Other modes are often considered as "premature" failures which should be avoided through proper design of the joint geometry and the composite material itself. Referring to the geometric dimensions such as specimen width, hole diameter and hole-to-edge distance, Collings [1] proposed ultimate bearing strength, net ultimate tensile strength and ultimate shear strength based on average stresses at failure, and the actual failure mode and load are associated with the one with the lowest load value among them. Fatigue damage around bolt holes

S.A. Nassar (✉) • X. Yang
Department of Mechanical Engineering, Fastening and Joining Research Institute (FAJRI), Oakland University, Rochester, MI 48309, USA
e-mail: nassar@oakland.edu

E. Patterson et al. (eds.), *Composite Materials and Joining Technologies for Composites, Volume 7: Proceedings of the 2012 Annual Conference on Experimental and Applied Mechanics,* Conference Proceedings of the Society for Experimental Mechanics Series 44,
DOI 10.1007/978-1-4614-4553-1_2,

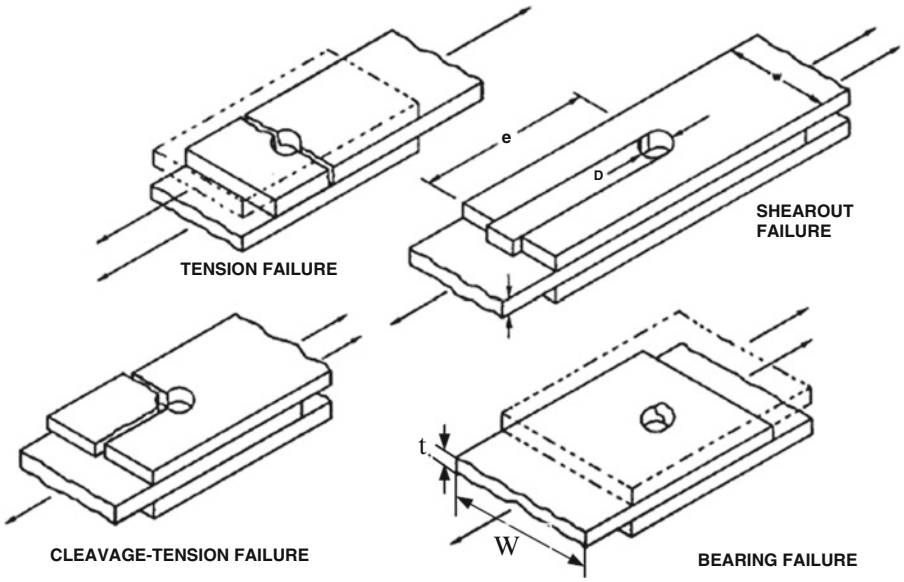

Fig. 2.1 Typical failure modes for bolted joints in composite laminate

consists of three types: hole wear, damage in the contact surface of the composite, and the growth of delamination around the bolt holes induced by the drilling. The hole wear is caused by the erosion of material around the bolt hole as a result of the friction forces. Damage at the contact surfaces is induced by bolt bending under loading. This would result in hole elongation during fatigue loading. It was found that the growth of delamination around bolt holes results in a decrease in the fatigue life of bolted joints. The failure load and pattern of composite bolted joints would obviously depend on the bolt preload level and distribution, orientation of layer reinforcing fibers, the ratio of bolt diameter to specimen width, bolt type, ratio of hole diameter to laminate thickness, number of bolts, and bolt arrangement.

Two problems should be addressed in the design of composite structures with joints that have multiple bolts. Firstly, it is necessary to adequately understand the behavior, strength, failure modes, and failure criterion of single-bolt joints. Secondly, it is necessary to accurately evaluate the loading magnitude and distribution. The strength prediction methods developed from single-bolt joints can also be utilized for determining the maximum failure load and the corresponding failure mode. The loading proportion is not generally equal for each fastener in the same joint. Therefore, determination of the ratio of loading proportion for each element becomes an important problem in the optimal design of joints with multiple threaded fasteners. Because this is mostly a highly statically indeterminate mechanical problem, FEA modeling is used for the determination of the loading ratio. Additionally, the FEA model can simulate the failure prediction based on the different failure criteria of the bearing, shear-out, and net-tension failure patterns.

An important consideration in joint testing and analysis is the selection of the type of test method with due attention to failure mode which is likely to lead to specific joint design requirements for a known composite system. The occurrence of a particular failure mode is primarily dependent on the joint geometry and laminate lay-up. Composite bolted joints may fail in various modes as shown in Fig. 2.1 [2]. The likelihood of a particular failure mode is influenced by bolt diameter D, laminate width w, edge distance e, and thickness t. The type of fastener used can also influence the occurrence of a particular failure mode.

For near-isotropic lay-ups in graphite/epoxy composite systems, net-section tensile/compressive failure occurs when the ratio of bolt diameter D to laminate width W is equal to or greater than one quarter (i.e. $D/w \geq 0.25$). It is characterized by failure of the plies in the primary load direction. Cleavage failure may initiate in the vicinity of the specimen end (rather than near the fastener); this mode of failure can be triggered by net-section failure. In some instances the bolt head may be pulled out through the laminate after the bolt is bent and/or deformed. Finally, it is important to note that for any given geometry, the failure mode may vary as a function of laminate lay-up and stacking sequence. Catastrophic failure modes such as tension, shear-out and cleavage-tension failures are avoidable through proper design of the joint geometry and the composite material itself. Most bolted composite structures are primarily designed to avoid bearing failure; investigating the effect of various joint parameters on bearing failure in a joint is of fundamental importance.

Adhesive joints increase structural efficiency and weight savings. They also minimize the potential for stress concentration within the joint, which cannot be achieved with mechanical fasteners. However, because of the lack of reliable, economical, and feasible inspection methods and due to the requirement for close dimensional tolerances in fabrication, designers have generally avoided bonded construction in primary structures. For bonded composite joints, the non-uniform stress distribution

along the bonding surface should always be accounted for. The peak stress is mainly dependent on the bonding pattern of the joint, bonded length, adhesive thickness, joint geometry, adherend stiffness imbalance, ductile adhesive response, and the composite adherends.

The main purpose of an adhesively bonded joint is to transfer loads in a reliable fashion under various environmental conditions throughout the entire service life of the joint and the parent structural component. The joint interfacial stresses introduced by those loads must remain essential part of the design, analysis, test, and validation process. Much of the current methodologies used in the design and analysis of adhesive joints in composite structures is based on the approach developed by L. J. Hart-Smith in a series of NASA-Langley-sponsored contracts [3, 4] during the early 1970s. Some of the key principles on which that effort was based on includes: (1) the use of simple 1-dimensional stress analysis of generic composite joints wherever possible [5]; (2) the need to select the joint design so as to ensure failure in the adherend rather than the adhesive, so that the adhesive is never the week link; (3) a recognition that the ductility of adhesives is beneficial in reducing the stress peaks in the adhesive; (4) careful use of such factors as adherend tapering to reduce or eliminate peel stresses from the joint; and (5) recognition of slow cyclic loading, corresponding to such phenomena as a major factor controlling durability of adhesive joints, and the need to avoid the worst effects of this type of loading by providing sufficient overlap length. This ensures that some of the adhesive is so lightly loaded that creep was not significant under the most severe scenarios of extreme humidity and temperature over the component service life. After Volkersen's work [6] on the stress analysis of a single lap joint, many analytical models have been proposed for stress analysis of various adhesively bonded joints. Sample 3-D analytical models for interfacial stress are developed by Ma et al. [7].

Most recently, several investigational studies have been carried out by Nassar et al. at the Fastening and Joining Research Institute-Oakland University, on various fastening and joining aspects of advanced composite materials. Experimental and analytical techniques, as well as FEA simulation, are used to study bolted joint behavior and failure modes different loading and temperature conditions. That includes deformation, NDE and preload control, Tribology of threaded fasteners, vibration and impact-induced loosening of preloaded threaded fasteners, elastic interaction, loss of preload, creep relaxation modeling, and hole and washer variables. Summary of the results from the work by Nassar et al. is presented in this paper.

2.2 Composite Bolting

Mechanical fasteners (bolts and rivets) require drilling of holes in composite materials, which ruptures the composite fiber reinforcements. Those holes generally cause stress concentration, but equally or even more significant is the increased probability for micro-cracks and local damage to be introduced around the holes, which can cause structural instability [8]. In spite of those draw backs, mechanical fastening of composites can still be a viable and proven joining option.

2.2.1 Effect of Geometry and Laminate Properties on the Bolt Bearing Behavior

For a single-bolt composite joint, the bolt hole diameter with clearance, laminate thickness, material, and layer stack sequences, washer, and clamping pressure all have significant effect on the bolt bearing behavior. The bearing stress σ_{br} and bearing strain ε_{br} are defined as follows

$$\sigma_{br} = \frac{P}{Dh} \tag{2.1}$$

$$\varepsilon_{br} = \frac{\delta_{coupon,bearing}}{D} \tag{2.2}$$

where P is applied load, D is bolt hole diameter, h is thickness of the laminate, and $\delta_{coupon,bearing}$ represents the deformation in the bolt hole. The typical bearing stress–strain curve for composite bolted joint coupon have three distinct regions as shown in Fig. 2.2: initial sliding, linear bearing response prior to the damage, and a nonlinear post damage stress region. The bearing stiffness is determined from the initial linear part of the curve. Figure 2.2 shows the definition of the bearing stiffness, the 2% offset bearing strength and ultimate strength.

Other researchers did some work on the effect of geometry and laminate properties on the bolt bearing behavior. Oh et al. [9] worked on bolted joints for hybrid composites made of glass-epoxy and carbon-epoxy under tensile loading.

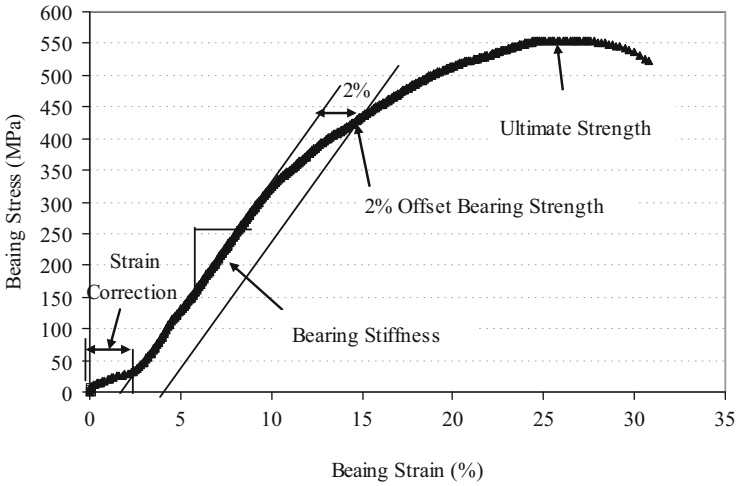

Fig. 2.2 Bearing stress–strain curve for bolted composite coupon

The design parameters investigated were laminate ply angle, stacking sequence, the ratio of glass-epoxy to carbon epoxy, the outer diameter of the washer and clamping pressure. Results showed that the peak load occurred before the maximum failure load due to the delamination of the laminate under the washer. The static test results of the hybrid composites with two kinds of stacking sequences revealed that the bearing strength increased as the $\pm 45^{\circ}$ plies were distributed evenly along the thickness direction irrespective of the joint material and the stacking pattern. The bearing strength increased as the bolt clamping pressure increased to 71.1 MPa, thereafter the bearing strength saturated to a constant value. The failure mode changed from bearing failure to tension failure when a 20 mm diameter washer was used.

Aktas and Dirikolu [10] carried out an experimental and numerical study on the strength of a pinned-joint made of carbon epoxy composite. The experimental results showed that when the ratio of the edge distance to the pin diameter (e/D) is $e/D \geq 4$and the ratio of the specimen width to the pin diameter (W/D) is $W/D \geq 4$, bearing failure was dominant, where as when the ratios were below 4, net tension, shear-out and mixed model failure were observed. The [90/45/-45/0]s joint configuration showed 20% higher bearing strength than the [0/45-45/90]s configuration.

McCarthy et al. [11] investigated the effect of hole clearance on the strength and stiffness of single-lap, single-bolt composite joint. Hole clearance had a significant effect on the joint stiffness and ultimate strain and less effect on the joint strength. The clearance caused a delay in load take up and this was considered to be a significant factor for multiple-bolt joint applications.

2.2.2 *Effect of Tightening Torque and Clamping Pressure on Bearing Behavior*

Girard et al. [12] studied the effect of stacking sequence and clamping pressure on the carbon/epoxy bolted composite joints. Bearing stress vs. hole elongation curves and the bearing stress vs. strain curves showed significant effect of clamping pressure on the initial bearing stress and the maximum bearing stress. Tightening the bolt increased the initial bearing stress by 22% and the maximum bearing stress by 105%. The increase in clamping pressure increased the post-peak stiffness, where as the initial stiffness and the bolt-hole elongation decreased significantly. The bearing stress vs. hole elongation curves showed that the angle of ply lay-ups had the lowest initial stiffness and the cross-ply lay-up had the highest initial and post peak stiffness. Orienting the fibers at an angle of 45° improved the bearing behavior. The results from the rosette strain gage positioned on the bearing zone showed a linear behavior for the angle-ply laminate, where as a nonlinear behavior was observed for the cross-ply and the quasi-isotropic lay-ups. This nonlinear behavior was mainly due to the stresses corresponding to the initiation of damage due to local delamination around the hole.

Park [13] investigated the effect of stacking sequence and clamping force on delamination bearing strength and ultimate bearing strength of mechanically fastened carbon/epoxy composite joints using an acoustic emission (AE) and load–displacement technique. The stacking sequence and the clamping pressure had a significant effect on the delamination and ultimate bearing strength of the mechanically fastened composite joint. An increase in clamping pressure increased the ultimate bearing strength to saturation, whereas the delamination bearing strength increased progressively. The clamping pressure suppressed the delamination and the interlaminar cracks. The failure mode changed from catastrophic fracture to a progressive failure as the clamping pressure was increased.

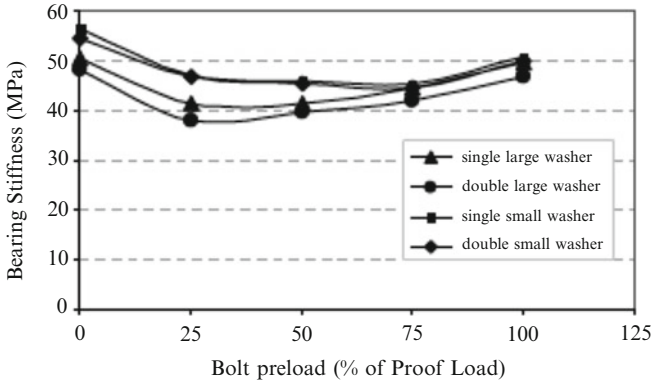

Fig. 2.3 Effect of bolt preload on joint bearing stiffness

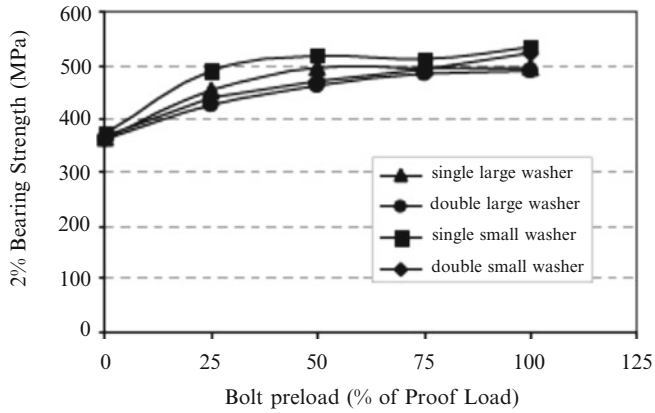

Fig. 2.4 Effect of bolt preload on offset bearing strength

Khashaba et al. [14] investigated the effect of bolt tightening torque and washer size on the bearing behavior of glass fiber reinforced epoxy composite ([0/±45/90]s) bolted joints. Damage analysis was carried out to understand the failure mechanism. Tightening torques of 0, 5, 10 and 15 Nm and the washer sizes of $D_{wo} = 14$, 18, 22, 27 mm were used in the study. The washer size of 18 mm and the tightening torque of 15 Nm produced the optimum clamping pressure. The composite bolted joints with 14 mm washers had higher clamping pressure but showed reduction in maximum bearing strength. The load–displacement curves of the finger tightened bolt joint showed least stiffness with non-linear behavior that indicated the unstable development of internal damage. Most of the tested specimens failed in a sequence, delamination, and net tension failure at 90° laminate, shear out failure at 0° layers and final failure which was nearly catastrophic due to the bearing failure of 45° layers.

2.2.3 Effect of Washers and Bolt Tension on the Behavior of Thick Composite Joints

Virupaksha and Nassar [15] studied the experimental characterization of thick composite bolted joints to explore the effect of washer size and bolt preload on bearing properties. S2-glass fabric-epoxy composite coupons [0/90; +45/−45@10sets] of 12.5 mm thickness were tested under double shear tensile loading. Two different washer sizes and thickness were used in the investigation. Five levels of bolt preload are investigated; namely, 0, 25%, 50%, 75% and 100% of the proof load of 1/2″−20 SAE Grade 5 fasteners. Figures 2.3, 2.4, and 2.5 show the effect of initial bolt load on the bearing joint stiffness, offset bearing strength, ultimate joint strength and joint strain for various joint configurations, respectively. The joint bearing stiffness was higher for the untightened bolted joint than that with much higher bolt preload (100% of proof load). The bearing stiffness was smallest for the joint with a preload equal to 25% of bolt proof load, and it increased with bolt preload. The offset bearing strength increased progressively with bolt preload. The ultimate joint strength was unaffected by increasing the bolt preload. Joint with small washers had higher bearing stiffness than those with large washers for initial bolt preload of 0%, 25% and 50%. Joints with small washers had higher offset bearing strength than the joints with large washers. The washer thickness had an insignificant effect on the ultimate joint strength and strain.

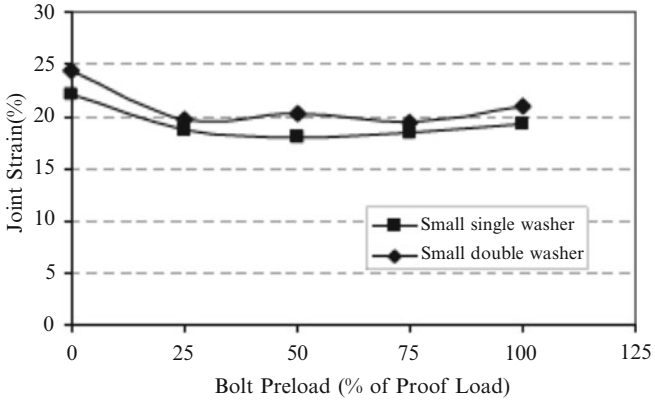

Fig. 2.5 Effect of bolt preload on joint strain

2.2.4 Vibration-Induced Loosening of Preloaded Threaded Fasteners

Threaded fasteners may have self-loosening when the joint is subjected to cyclic shear loads. The self-loosening leads to the partial loss or complete loss of the clamp load so that the function of the fastener will lose. When the clamp load loses completely, the bolt will sustain the whole separating force fluctuation under the cyclic separating force. This may result in the bolt fatigue failure much more easily. The shear force cannot be transferred between the two clamped joint members by using the friction force on the contact surfaces when the clamp load is zero. If the clamp load of the gasketed bolted joints loses, the leakage will occur. Therefore, the loss of the clamp load is one of the common failure modes of threaded fastener. There have been some studies on the self-loosening of threaded fasteners; most of them are experimental. Junker [16] studied the effect of the transverse vibrations on the self-loosening of threaded fasteners and showed that the loosening of threaded fasteners was far more severe when the joint was subjected to transverse cyclic loads. On the other hand, Junker designed a test machine for the self-loosening as shown in Fig. 2.6. In his work, he concluded that the self-loosening happens when slippage took place between engaged threads and/or under the bolt head/nut.

Based on the relative kinetic relationships as shown in Figs. 2.7 and 2.8 on the bearing surface and thread surface, Nassar and Yang [17] proposed the formulations for the sliding bearing friction torque and thread friction torque as shown in the following:

$$R_{Tb} = \left|\frac{T_b}{\mu_b q_{b0}}\right| = \int_{r_i}^{r_e} r^2 dr \int_0^{2\pi} \frac{(\eta_b \sin\theta + r)d\theta}{\sqrt{{\eta_b}^2 + 2\eta_b r \sin\theta + r^2}} \tag{2.3}$$

$$R_{Fb} = \left|\frac{F_{bs}}{\mu_b q_{b0}}\right| = -\int_{r_i}^{r_e} r dr \int_0^{2\pi} \frac{(\eta_b + r \sin\theta)d\theta}{\sqrt{{\eta_b}^2 + r^2 + 2\eta_b r \sin\theta}} \tag{2.4}$$

$$R_{Tt} = \left|\frac{T_t}{\mu_t q_{t0}}\right| = \sqrt{\sec^2\alpha + \tan^2\beta} \int_{r_{\min}}^{r_{maj}} r^2 dr \int_0^{2\pi} \frac{[r - \eta_t \sin\theta]d\theta}{\sqrt{\eta_t^2(1 + \tan^2\alpha\cos^2\theta) + r^2 - 2\eta_t r \sin\theta}} \tag{2.5}$$

$$R_{Ft} = \left|\frac{F_{ts}}{\mu_t q_{t0}}\right| = \sqrt{\sec^2\alpha + \tan^2\beta} \int_{r_{\min}}^{r_{maj}} r dr \int_0^{2\pi} \frac{(\eta_t - r \sin\theta)d\theta}{\sqrt{\eta_t^2(1 + \tan^2\alpha\cos^2\theta) + r^2 - 2\eta_t r \sin\theta}} \tag{2.6}$$

where T_b is the bearing frictional torque, F_{bs} is transverse bearing friction shear force, $\eta_b = v_{b1}/\omega_b$ is the bearing translation-rotational ratio, $v_{b1}$is the relative translation velocity along x direction, ω_b is the relative rotation angular velocity of the bolt underhead to the joint member, μ_b is bearing friction coefficient, and q_{b0} is the average bearing contact pressure. T_t is the thread friction torque, μ_t is the thread friction coefficient, and q_{t0} is the average thread contact pressure, and F_{ts} is transverse thread friction shear force, $\eta_t = v_{tx}/\omega_t$ is the thread translation-rotational ratio, $v_{tx}$is the relative thread translation velocity

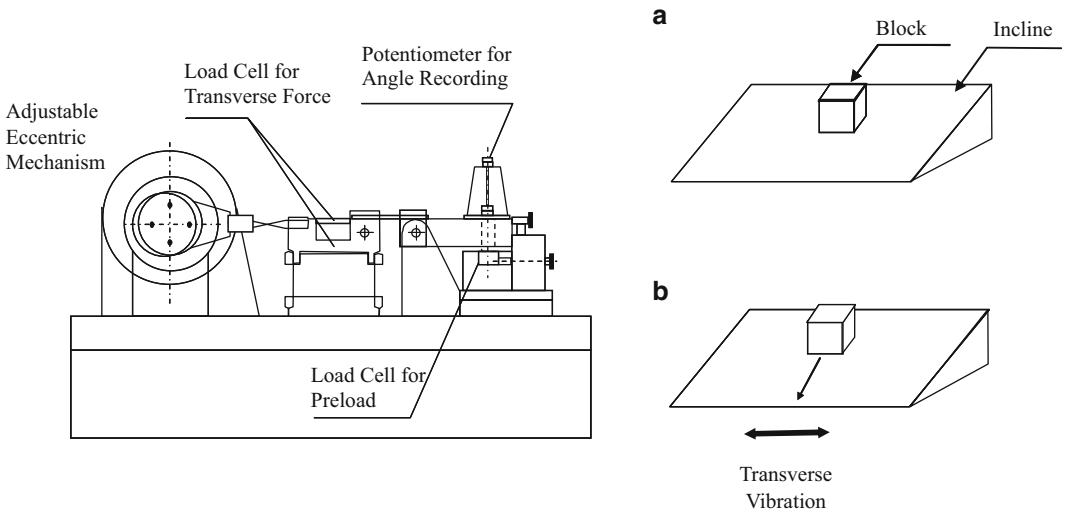

Fig. 2.6 Junker machine for self-loosening test; schematic of the block slippage due to vibration

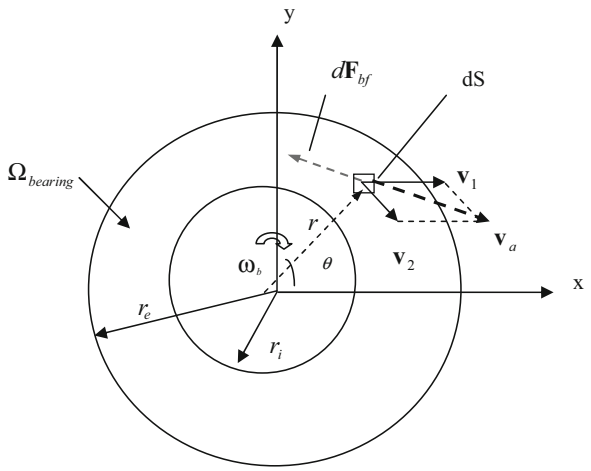

Fig. 2.7 The relative movement on the underhead bearing surface to the joint member

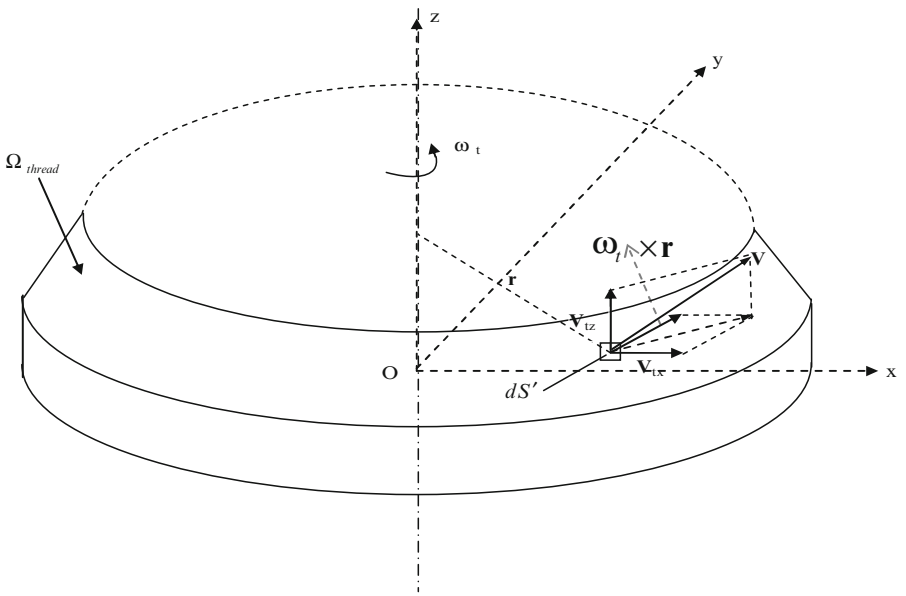

Fig. 2.8 Schematic relative movement of thread surface

along x direction, ω_t is the relative rotation angular velocity of the bolt thread to the joint member, and α is the half of the thread profile angle and β is lead helix angle.

From Eqs. 2.3, 2.4, 2.5, and 2.6, the sliding bearing and thread friction torque, the sliding bearing and thread shear force are dependent on the ratio of the relative transition movement to the rotation velocity of the bolt. When there is only the rotation velocity, the sliding friction torques are corresponding to the ones under bolt tightening and the resultant shear force is zero. When there is only relative transition movement, the sliding friction torques are zero.

When the pitch torque is larger than the sum of the sliding bearing friction torque and the sliding thread friction torque, the self-loosening occurs. Based on the dynamic movement equations of the bolted joint, the self-loosening under transverse cyclic loading can be predicted. Nassar and Housari [18, 19], Housari and Nassar [20] investigated the effect of thread pitch, initial bolt tension, hole clearance thread fit, bearing and thread friction, and amplitude of the cyclic transverse load on the loosening of threaded fasteners. They concluded that these parameters have a significant effect on the self-loosening of threaded fasteners. Yang and Nassar [21] developed a mathematical model for self-loosening of bolted joint under transverse cyclic loading, and Yang et al [22] proposed a criterion for preventing self-loosening under some specific conditions.

Following a different research route, Shoji and Sawa [23] proposed a 3-Dimensional finite element model to simulate the mechanism of the self-loosening caused by the relative slippage. Their simulation results show that during one cycle the nut rotates in both the tightening and the loosening directions with net rotation in the loosening direction. Independently, Jiang et al. [24] proposed a three dimensional elastic–plastic finite element model to investigate the early stage of self-loosening caused by the plastic ratcheting deformation of the thread roots, which does not include rotation of the bolt or the nut. After the bolt tightening, the micro-plastic deformation of the asperities on contact area occurs under the transverse cyclic loading. On the other side, the misalignment of the bolt assembly will be gradually adjusted in the initial cycles. Those lead to the initial clamp load loss. When the contact interfaces have relative movement, the wear of the contact area will decrease the bolt elongation and the joint compression, and it will change the surface roughness and the hardness conditions of the contact areas. The bolt elongation decrease results in the clamp load loss. The surface roughness and hardness change will make the friction coefficient on the contact area change with the transverse cyclic loading. As this phenomenon is affected by lots of parameters, quantitative results are still very scarce.

2.2.5 Elastic-Interaction of Multi-bolted Joints During Tightening

Nassar and Alkelani [25, 26] carried out the elastic-interaction of gasketed joints. Elastic interaction between the various fasteners in gasketed flanged joints is significantly influenced by the gasket material and thickness, bolt spacing, and by the tightening strategy and sequence. For the same tightening torque level, using simultaneous tightening of all bolts produces a higher and more uniform clamp load in the joint. Simultaneous tightening has also reduced the amount of tension drop off due to the combined effect of elastic interaction and gasket creep relaxation. The fastener grip length had insignificant effect on the clamp load loss for soft gaskets (e.g. red rubber). The residual clamp load level in gasketed joints was significantly affected by the gasket material used in the joint (i.e. soft versus hard gaskets). When a soft gasket was used in the joint, it was observed that increasing the tightening speed significantly has reduced the average residual clamp load in the joint; that was likely due to the continued gasket creep relaxation after the high-speed tightening process had been completed. Conversely, for a hard gasket (e.g. flexible graphite), it was observed that increasing the tightening speed increased the residual clamp load in joint. The study showed that simultaneous tightening of all bolts produced both higher initial and higher residual clamp loads, as compared to a star pattern tightening of the individual bolts. Using a second tightening pass increased the residual clamp load more for the individual bolt tightening as compared to simultaneous tightening of all bolts in the joint. Elastic interaction between preloaded bolts in the same joint was significantly increased by increasing the thickness of a soft gasket (styrene butadiene rubber), while the thickness of a hard gasket (flexible graphite) has not significantly affected the elastic interaction.

Alkelani et al. [27, 28] proposed a closed form mathematical modeling of elastic interaction and creep relaxation for the clamp load as a function of the time elapsed after the initial tightening of the joint as shown in Figs. 2.9 and 2.10. Gasket constants are found to be independent of the gasket stress level, but are affected by the gasket thickness for the gasket material considered in this study (red rubber). The bolt tension loss as a percentage of bolt preload does not depend on the fastener preload level. Fastener preload level has insignificant effect on elastic interaction. The clamp load formulation has been successfully used to determine the required initial clamp load level that is necessary to provide the desired level of a steady state residual clamp load in the joint, by taking the gasket creep relaxation into account. The good agreement between the mathematical model results and the experimental data suggests that the proposed model can be used to accurately describe the gasket behavior and the clamp load loss due to gasket creep relaxation. The amount of elastic interaction is

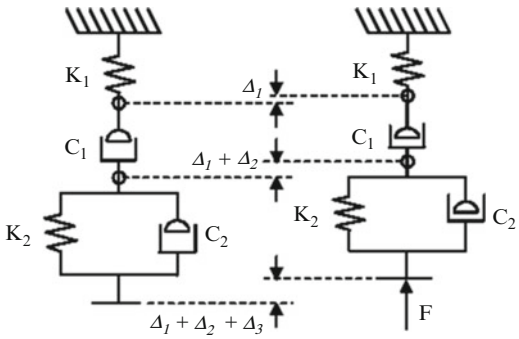

Fig. 2.9 Mechanical model of a typical gasket

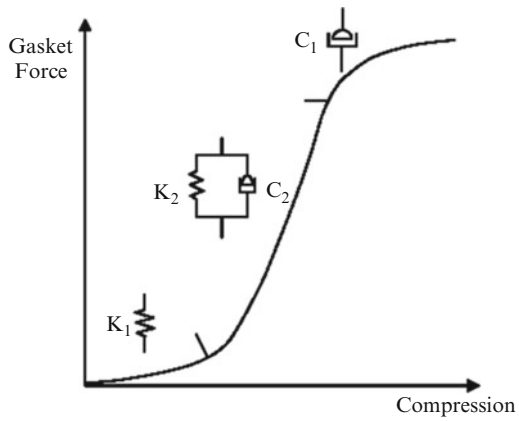

Fig. 2.10 Gasket Force-Compression

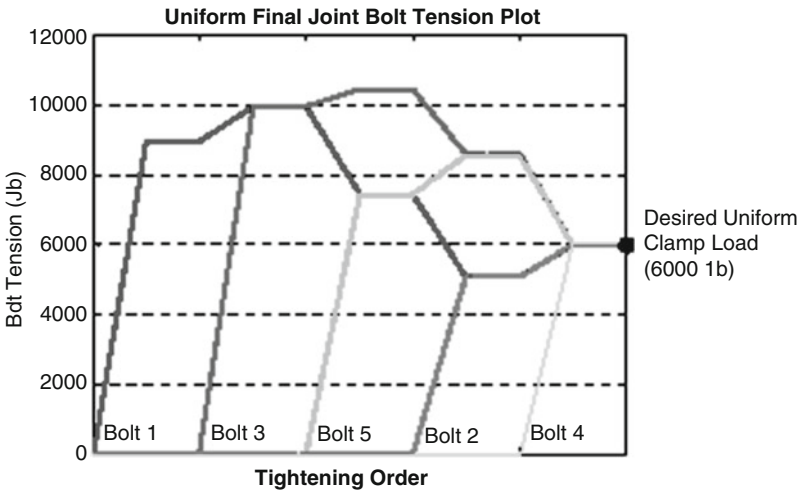

Fig. 2.11 Model prediction of a desired uniform clamp load

increased by increasing the gasket thickness. Reducing bolt spacing causes more loss of bolt tension due to increased elastic interaction. The final clamp load level and uniformity is significantly influenced by the tightening pattern. Good agreement exists between the proposed model and the experimental results as shown in Figs. 2.11 and 2.12. Hence, the model can reliably be used to predict and/or achieve a uniform clamp load distribution in flat-faced flanged joint.

Nassar et al. [29] did FEA simulation to Study the Effect of Multi-Pass Tightening of Gasketed Bolt Joint. The FEA model is shown in Figs. 2.13 and 2.14 shows the experimental and FEA results for multi-pass star tightening. For gasketed joint, the finite element simulation results have a good agreement with the experimental ones. The finite element simulation methodology can be used to develop bolting procedures for any bolted joint assembly. Four-pass sequential and star tightening operation is enough to achieve uniform preloads for the 5-bolt gasketed joint model. The experimental and the FE simulated results show that the multi-pass tightening strategy is very effective for the uniformity of the bolt tensions of

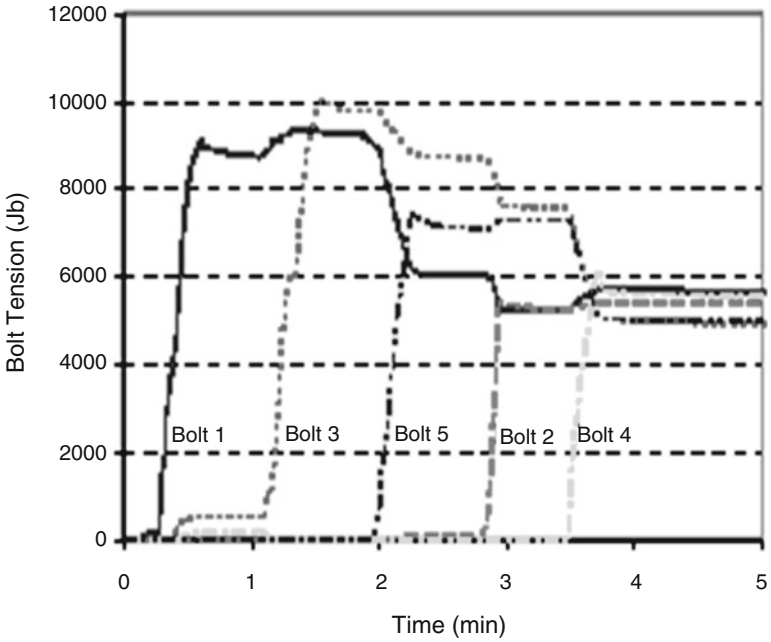

Fig. 2.12 Experimental verification of model prediction of a desired uniform clamp load

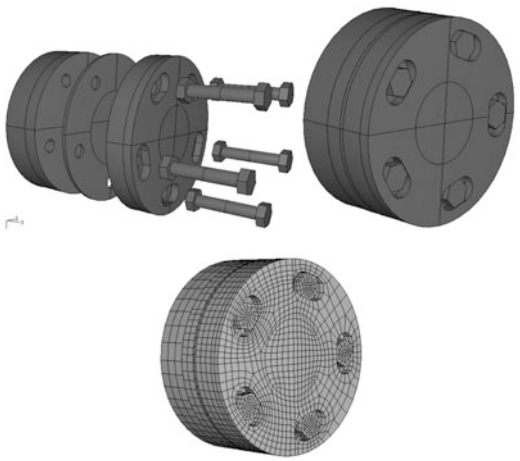

Fig. 2.13 Finite element models

the gasketed joint. The scatter of bolt load for the star pattern tightening is much higher than that for the sequential tightening with the same target preload at the end of each pass. For both of tightening patterns, the effect of the tightening history on the bolt tension variation of the subsequential tightening very significantly even though the previous tightening was completely removed before the subsequential tightening. It is easier to achieve uniform preload for the lower level of target preload with multi-pass sequential tightening procedure for the flexible graphite gasketed joint. The single pass tightening approach with the linear elastic gasket for the uniformity of bolt tensions was proposed, and the approach has been verified by FEA simulation.

2.3 Adhesively Bonded Composite Joints

This section highlights some of the recent analytical and experimental investigations of the behavior of bonded laminated joints under mechanical and thermo-mechanical loads.

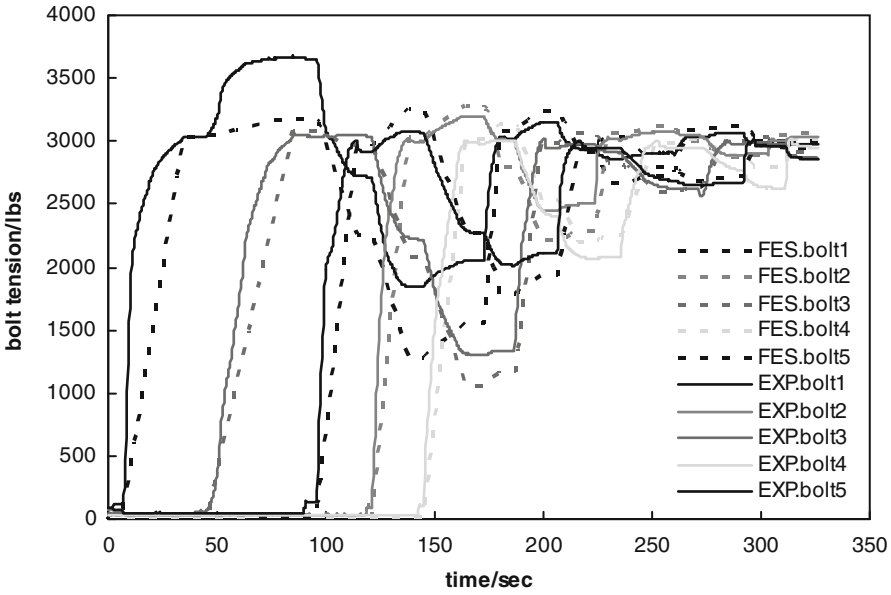

Fig. 2.14 The experimental and simulated bolt tension variations of gasketed joint in the Multi-pass star tightening with the preload of 3,000 lb

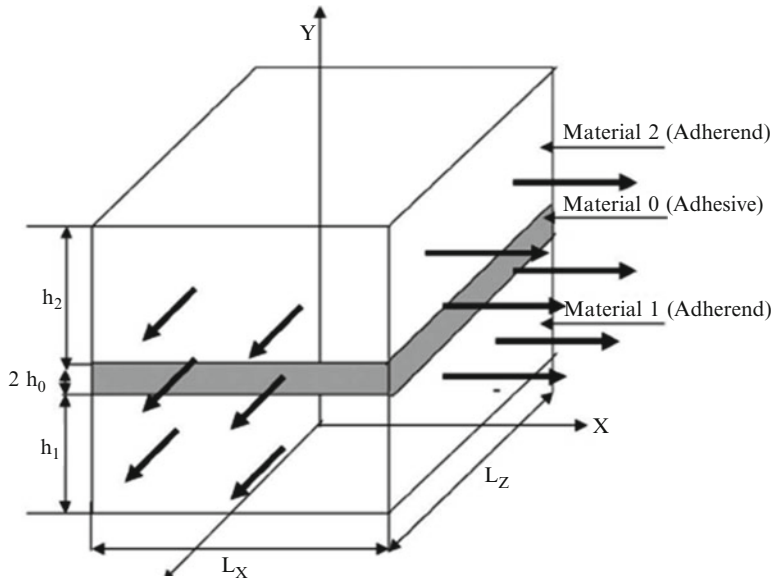

Fig. 2.15 Complete model of adhesive bonded joint

2.3.1 Interfacial Stresses in Adhesively Bonded Joints

Nassar and Virupaksha [30] introduced a linear continuum mixture model of periodically-stacked laminates with adhesive bonding. They derived a set of partial differential equations for interfacial shear stresses on both sides of a representative adhesive layer using the 3-D multi-layer model shown in Fig. 2.15. Analytical expressions were obtained for the interfacial shear stresses under thermo-mechanical loading. The numerical results on the model show that increasing the thickness of the adhesive causes a significant increase in the interfacial shear stresses; the larger difference in the elastic and thermal properties between the adhesive and the layered adherend leads to the higher corresponding interfacial shear stress.